JOURNAL OF GEOPHYSICAL RESEARCH, VOL. 106, NO. 12, PAGES 30771–30782, DECEMBER 10, 2001

Multiparameter two-dimensional inversion of scattered teleseismic body waves 1. Theory for oblique incidence

M. G. Bostock, S. Rondenay,[1] and J. Shragge[2]

Department of Earth and Ocean Sciences, University of British Columbia, Vancouver, British Columbia, Canada

Abstract. This is the first paper in a three-part series that examines formal inversion of the teleseismic *P* wave coda for discontinuous variations in elastic properties beneath dense, three-component, seismic arrays. In this paper, we develop the theoretical framework for a migration method that draws upon the tenets of inverse scattering theory and is amenable to practical implementation. The forward problem is formulated for two-dimensional (2-D) heterogeneity in observance of formal sampling requirements and currently accessible instrumentation. A ray theoretic Green's function, corresponding to a line source with axial component of forcing, is employed within the 2-D Born approximation to accommodate planar, incident wave fields at arbitrary back azimuths. Both the forward scattered response generated by the upgoing incident wave field and the backscattered response created by its reflection at the free surface are included within the formulation. In accordance with the high-frequency and single-scattering approximations employed in the forward problem the inverse problem is cast as a generalized Radon transform. The resulting back projection operator is well suited to the teleseismic context in several respects. It is tolerant of irregularities in array geometry and source distribution and allows a full complement of global seismicity to be utilized through its accommodation of oblique incidence. By permitting both independent and simultaneous treatment of different scattering modes (reflections, transmissions, conversions) the inversion formula facilitates a direct appraisal of individual mode contributions to the recovery of structure. In particular, it becomes evident that incorporation of backscattered modes leads to (1) a better localization of structure than possible using forward scattered energy and (2) the imposition of complementary constraints on elastic properties.

1. Introduction

Multichannel processing of teleseismic body wave data is becoming an increasingly important component of crustal and upper mantle structural studies. The *P* wave field is particularly useful in this regard owing to its relatively high signal-to-noise ratio and broad signal bandwidth, characteristics which afford it considerably greater resolving power than other teleseismic phases. Although *P* wave travel time tomography has been the most widely exploited technique to date for unveiling lateral heterogeneity within the lithosphere and underlying mantle [e.g., *Aki et al.*, 1977; *VanDecar*, 1991; *Humphreys and Dueker*, 1994], there is a growing appreciation of the potential that secondary scattered waves in the *P* coda harbor for delineation of still finer structural variations. This is evidenced through a range of studies undertaken in recent years involving multichannel processing of scattered teleseismic waves for crustal [*Revenaugh*, 1995b; *Ryberg and Weber*, 2000], lithospheric [*Kosarev et al.*, 1999; *Revenaugh*, 1995a], and transition zone structure [*Dueker and Sheehan*, 1997; *Shearer et al.*, 1999]. With the projected availability of greatly increased numbers of portable broadband, three-component seismometers [e.g., *Levander et al.*, 1999], further developments in multichannel processing of scattered teleseismic phases hold the promise of exciting new insights into the nature of the lithosphere and underlying mantle.

This paper is the first of a three-part series that investigates formal, yet practical, inversion of teleseismic scattered waves for crust and upper mantle structure. It is based on a theory of inverse scattering developed by Beylkin and coworkers [*Beylkin*, 1985; *Miller et al.*, 1987; *Beylkin and Burridge*, 1990] for seismic reflection applications, which exploits an analogy between high-frequency, single scattering and the Radon transform. The present work differs from these previous studies primarily through the geometrical context of the teleseismic application and an attempt to incorporate free-surface multiple reflections within the inverse problem. It also extends a previous study by *Bostock and Rondenay* [1999] (hereinafter referred to as BR) that considered teleseismic body waves recorded on strictly linear receiver arrays oriented perpendicularly to local geologic strike and in the plane of sources. This latter formulation, while insightful, is of limited practical use because (1) a majority of global seismicity is unavailable for analysis due to the irregular distribution of earthquakes along plate boundaries and (2) logistical considerations, e.g., road access, often dictate array geometries with uneven sampling and an obliquity to local geologic strike. The present study overcomes both of these shortcomings and thereby allows consideration of field data sets.

We will generalize the problem considered by BR as follows. The requirement of dense spatial sampling (i.e.,

[1]Now at Department of Geological Sciences, Brown University, Providence, Rhode Island, USA.

[2]Now at Hager GeoScience Inc., Woburn, Massachusetts, USA.

Paper number 2001JB000330.
0148-0227/01/2001JB000330$09.00

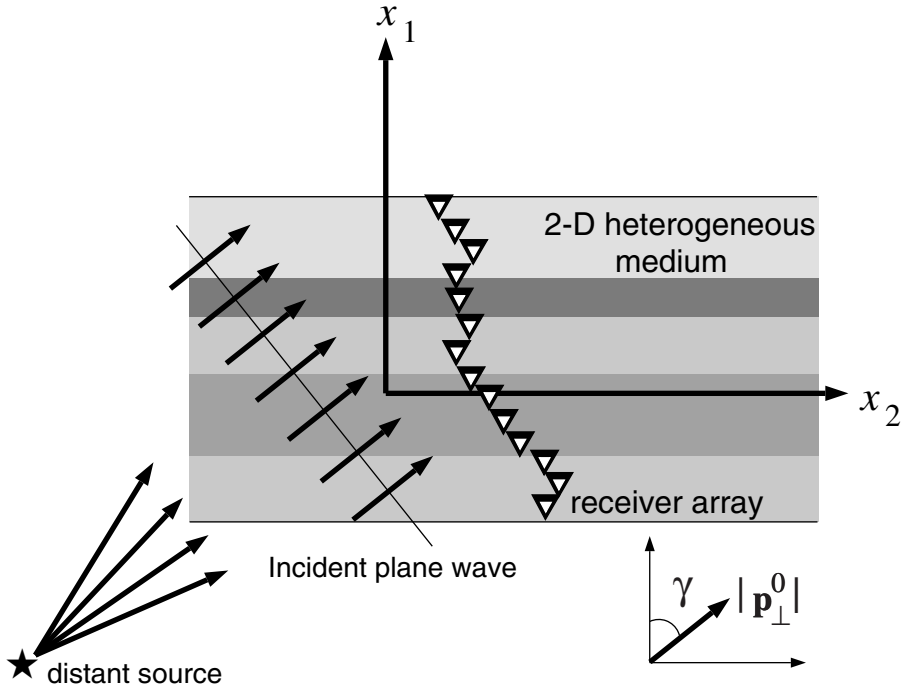

Figure 1. Plan view of geometry for a teleseismic wave field incident upon a 2-D receiver-side crust and upper mantle. The incident wave front is assumed to be planar in horizontal aspect with horizontal slowness $\mathbf{p}_\perp^0 = [p_1^0, p_2]^T$. Snell's law requires that the component of slowness in the strike direction, p_2, be conserved across all scattered waves for an individual incident wave field. Note that receiver responses measured at constant x_1 are identical to within a phase shift of $e^{-i\omega p_2 x_2}$. Further note that x_1, x_3 is a plane of mirror symmetry; hence the integration over back azimuth, γ, in (39) may be restricted to the interval [0°, 180°].

station spacings of ~5 km or less to avoid aliasing higher frequencies within the teleseismic *P* wave field) and currently accessible recording infrastructure restrict our consideration to quasi-linear arrays of receivers. By quasi-linear we imply that some deviation from a strictly linear configuration can be tolerated, as indicated in Figure 1. Because the two-dimensional (2-D) Earth's surface is effectively sampled in only one dimension, the inverse problem of retrieving 3-D subsurface structure is highly underdetermined. Consequently, we will regularize the problem by assuming that the underlying Earth is 2-D with known geologic strike. While it is desirable that strike direction be perpendicular to the dominant array axis to mitigate the effects of true 3-D structure, this is not strictly required in the treatment that follows. Furthermore, to exploit the full complement of sparsely distributed earthquake sources (and thereby render the treatment practically useful), we must allow for wave fields incident upon the underlying crust and mantle from arbitrary back azimuths.

The large (>30°) epicentral distances represented by the teleseismic *P* wave field permit an important, simplifying assumption to be made, that is, that the incident wave field is effectively planar in horizontal aspect over the breadth of the array. As the incident wave field encounters small-scale structures, it generates forward scattered waves that follow the direct wave to the surface. For single-station recordings, these waves are often interpreted in terms of near-planar, lithospheric discontinuities in shear velocity using the receiver function technique [*Langston*, 1979; *Vinnik*, 1977]. The forward scattering geometry contrasts with that of seismic exploration practice where a reflection or backscattering response is generally measured (see Figure 2). It is important to recognize, however, that the teleseismic wave field also affords the opportunity of measuring a backscattered response through the readily predictable reflection of an incident plane wave at the free surface. These reflections can be regarded as new plane wave sources that further interact with underlying structure to produce backscattered energy recorded on the receiver array. Although this surface-reflected energy is frequently regarded as a source of noise, our approach will be to include it together with forward scattered energy in a simultaneous inversion for subsurface structure.

We will begin by developing the forward problem using a single-scattering/high-frequency formulation which describes the forward scattering of a plane wave obliquely incident from below upon a 2-D medium (equations (24) and (25)). Having cast the forward problem in a standard form, we proceed to identify an approximate inversion formula (equations (39)–(41)) for isotropic material property perturbations using the generalized Radon transform as from *Miller et al.* [1987] and *Beylkin and Burridge* [1990]. Note that our derivation for both forward and inverse problems is similar in outline to these two earlier studies. Consequently, emphasis in this paper is placed on those aspects specifically relevant to the teleseismic application. We then proceed to examine the effect of the free surface; in particular, we demonstrate how free-surface reflections may be readily accommodated within the formalism to provide additional constraints on subsurface structure. Our treatment concludes with a brief discussion of factors governing the resolution of physical and geometrical properties of interest. This paper (hereinafter referred to as paper 1) establishes the theoretical framework and background for the two companion papers by *Shragge et al.* [this issue] (hereinafter referred to as paper 2) and *Rondenay et al.* [this issue] (hereinafter referred to as paper 3). Paper 2 examines the potential and limitations of our approach using complete synthetic seismograms for an idealized collisional suture model. Paper 3 completes the three-part series

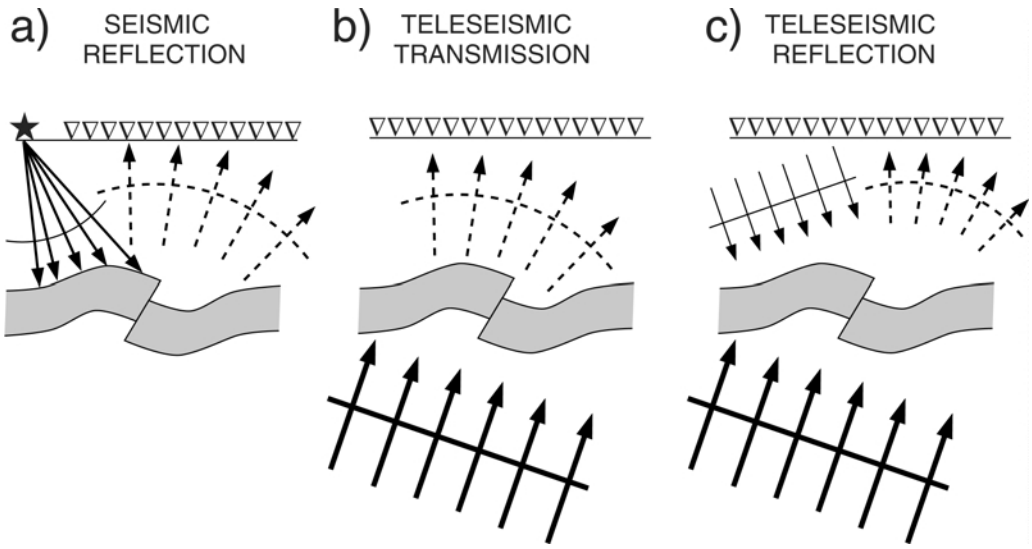

Figure 2. Scattering geometries. (a) Backscattering geometry for seismic reflection profiling. A point source produces waves that are reflected from underlying structure and recorded at an array of receivers at the surface. (b) Forward scattering geometry for passive teleseismic experiment. Quasi-planar teleseismic wave field incident upon structure from below generates transmitted waves recorded at receivers on the surface. (c) Backscattering geometry for passive teleseismic experiment. Quasi-planar surface-reflected P and S wave fields are topside reflected from structure and recorded at surface receivers.

with an example of processing that uses field data from the Cascadia 1993–1994 (CASC93) teleseismic experiment [*Li and Nabelek*, 1999].

2. Forward Problem

Consider the scenario depicted in Figure 1. A slightly irregular configuration of receivers is oriented obliquely to the strike (taken to be the x_2 direction) of an underlying, depth-localized 2-D medium. These receivers record the teleseismic wave field originating from a distant earthquake source at some arbitrary back azimuth γ. In the following derivation we will assume that propagation from source to receiver-side upper mantle occurs within a 1-D reference medium and that local 2-D, receiver-side, crust and mantle structure exists as a perturbation on this 1-D medium, as shown in Figure 3. We shall assume that the Earth's sphericity has been accounted for in advance through an Earth-flattening transformation [*Chapman*, 1973], if necessary. The invariance of material properties in the x_2 direction implies that wave number components of the incident wave field in this direction scatter independently, that is, without cross coupling. For sources at teleseismic distances the incident wave field can be taken to be effectively planar in horizontal aspect and thus characterized by a single horizontal slowness. Consequently, all scattered waves will share this same component of slowness in the x_2 direction for any individual source. This behavior, an expression of Snell's law for 2-D geometries, is the essential ingredient in the treatment of the forward problem.

Upon Fourier transformation in time the total displacement wave field u_i in a 2-D anisotropic elastic medium can be expressed in indicial notation as

$$\partial_j\left(c_{ijkl}\partial_l u_k\right) + \rho\omega^2 u_i = -F_i, \tag{1}$$

where $c_{ijkl} = c_{ijkl}(x_1, x_3)$ is the elastic tensor, $\rho = \rho(x_1, x_3)$ is density, ω is radial frequency, F_i is body force per unit volume, and, e.g., ∂_j is an abbreviation for $\partial/\partial x_j$. To simplify the ensuing development, we will represent this equation in operator notation as

$$L_{ik}u_k = -F_i, \tag{2}$$

where the second-order, linear differential operator L_{ik} is defined by

$$L_{ik} = \partial_j c_{ijkl}\partial_l + \rho\omega^2\delta_{ik}. \tag{3}$$

The reference displacement wave field u_i^0 satisfies a similar equation:

$$L_{ik}^0 u_k^0 = -F_i, \tag{4}$$

but with material properties replaced by $c_{ijkl}^0 = c_{ijkl}^0(x_3)$ and $\rho^0 = \rho(x_3)$ which, recall, we have restricted to be functions of depth alone. The definition of perturbation quantities

$$\Delta u_i = u_i - u_i^0 \tag{5}$$

$$\Delta L_{ik} = L_{ik} - L_{ik}^0, \tag{6}$$

leads to the derivation of a wave equation for the "scattered" displacement field Δu_k,

$$L_{ik}^0 \Delta u_k = -\Delta L_{ik} u_k, \tag{7}$$

where Δu_k can be interpreted as arising from an effective source distribution involving material property perturbations $\Delta c_{ijkl}(x_1, x_3)$, $\Delta\rho(x_1,x_3)$, and the total wave field $u_i(x_1, x_2, x_3)$. Equation (7) is then Fourier transformed to remove the dependence on coordinate x_2, yielding

$$\widetilde{L}_{ik}^0 \Delta\widetilde{u}_k = -\Delta\widetilde{L}_{ik}\widetilde{u}_k, \tag{8}$$

where the transformed quantities are identified through an overlying tilde. The dual variable (i.e., wave number in the x_2 direction) is represented as ωp_2 with p_2 equal to the component of phase

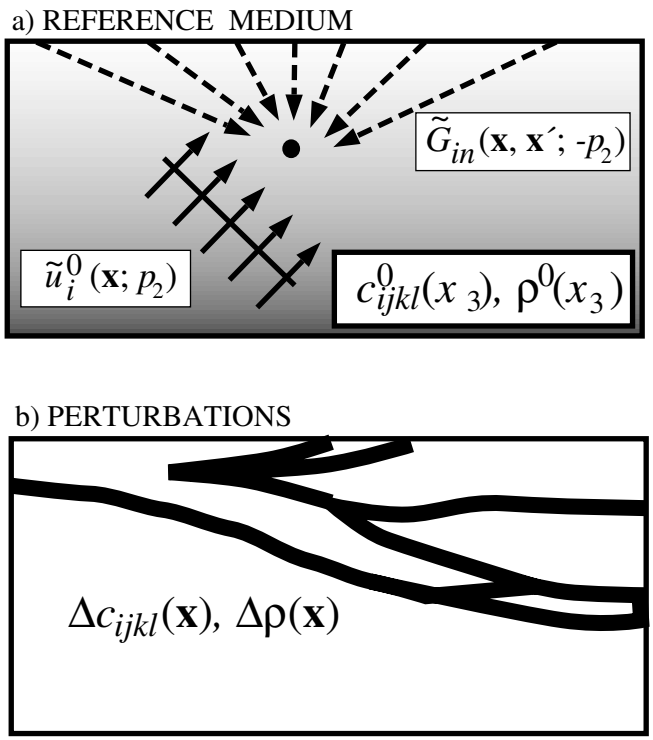

Figure 3. Schematic breakdown of Earth into (a) reference medium and (b) perturbations in the Born formulation of the forward problem. All propagation takes place within the known, smoothly varying reference medium where elasticity and density are functions of depth alone. The unknown perturbations in elasticity and density represent 2-D varying, short-wavelength structure within the Earth.

slowness in the x_2 direction; thus all transformed quantities possess the same dependency $(x_1, x_3; p_2)$.

We now introduce the adjoint Green's function $\widetilde{G}^{\dagger}_{kn} = \widetilde{G}^{\dagger}_{kn}(x_1, x_3; x_1', x_3'; p_2)$ that satisfies

$$\widetilde{L}^{0\dagger}_{ik}\widetilde{G}^{\dagger}_{kn} = -\delta_{in}\delta(x_1 - x_1')\delta(x_3 - x_3'), \tag{9}$$

where the primed coordinates denote the source location and the operator $\widetilde{L}^{0\dagger}$ is adjoint to $\widetilde{L}^0$. The derivation proceeds by taking the inner product of (8) with $\widetilde{G}^{\dagger}_{in}$ and (9) with $\Delta\widetilde{u}_i$, subtracting, integrating over the x_1, x_3 plane, and applying the divergence theorem. Noting that $\widetilde{G}^{\dagger}_{in}$ and $\Delta\widetilde{u}_i$ satisfy outgoing radiation conditions such that the resulting surface integrals vanish [see, e.g., *Hudson*, 1980], we have

$$\Delta\widetilde{u}_n(x_1', x_3'; p_2) = \int\int dx_1 dx_3 \widetilde{G}^{\dagger}_{in}\Delta\widetilde{L}_{ik}\widetilde{u}_k. \tag{10}$$

The adjoint Green's function satisfies

$$\begin{aligned}\widetilde{G}^{\dagger}_{in}(x_1, x_3; x_1', x_3'; p_2) &= \widetilde{G}_{ni}(x_1', x_3'; x_1, x_3; p_2)\\ &= \widetilde{G}_{in}(x_1, x_3; x_1', x_3'; -p_2)\end{aligned} \tag{11}$$

where $\widetilde{G}_{in}$ is the Green's function for the operator $\widetilde{L}^0$. The first equality follows from the definition of the adjoint Green's function, while the second is a result of the geometry adopted for this problem. In addition, we have assumed that the perturbations $\Delta c_{ijkl}(x_1, x_3)$, $\Delta\rho(x_1, x_3)$ vanish at the free surface and that there are no discontinuities in material properties in either the reference medium or the 2-D perturbation structure. The presence of discontinuities will produce additional interface terms in (10), which may be cancelled through an integration by parts of the right-hand side. The harmonic dependencies in x_2 of the wave fields within the integrand are therefore reinstated to allow a compact expansion of the operator, and the integral is evaluated by parts to yield

$$\Delta\widetilde{u}_n = \int\int dx_1 dx_3 - \Delta c_{ijkl}\partial_l u_k \partial_j G^{\dagger}_{in} + \Delta\rho\omega^2 u_i G^{\dagger}_{in}, \tag{12}$$

where, explicitly,

$$u_k = u_k(x_1, x_3; x_2) = \widetilde{u}_k(x_1, x_3; p_2)e^{i\omega p_2 x_2} \tag{13}$$

$$G^{\dagger}_{in} = G^{\dagger}_{in}(x_1, x_3; x_1', x_3'; x_2) = \widetilde{G}_{in}(x_1, x_3; x_1', x_3'; -p_2)e^{-i\omega p_2 x_2}. \tag{14}$$

Note that we have used the properties of the adjoint Green's function (i.e., second equality in (11)) to transfer the ∂_2 operator from $\Delta c_{ijkl}\partial_l u_k$ to $G^{\dagger}_{in}$ in (12). Equation (12) is now in the form of a Lippman-Schwinger equation and can be linearized through the Born approximation ($u_k \approx u^0_k$) under the assumption that perturbations in material properties are small, yielding

$$\Delta\widetilde{u}_n = \int\int dx_1 dx_3 - \Delta c_{ijkl}\partial_l u^0_k \partial_j G^{\dagger}_{in} + \Delta\rho\omega^2 u^0_i G^{\dagger}_{in}. \tag{15}$$

Equation (15) applies for general anisotropy and treatment thereof in a 2-D context is reasonable since many of the processes inferred to impart anisotropy to the lithosphere and upper mantle (e.g., ridge spreading, plate decoupling, subduction) are inherently 2-D. However, unless seismicity is well sampled in back azimuth and arrays are deployed for longer durations (i.e., several years at least), it is unlikely that field data sets will be adequate for analysis of anisotropy. In the present work, we will therefore proceed to confine our attention to purely isotropic heterogeneity,

$$\Delta c_{ijkl} = \Delta\lambda\delta_{ij}\delta_{kl} + \Delta\mu(\delta_{ik}\delta_{jl} + \delta_{il}\delta_{jk}). \tag{16}$$

In addition, we will restrict consideration to the treatment of waves scattered from incident teleseismic *P*, since it is likely to be more useful in the retrieval of mantle structure than teleseismic *S* for a range of reasons which include (1) lower signal-generated noise levels, (2) higher frequency content, (3) lower horizontal slowness leading to diminished likelihood of supercritical interactions in subhorizontally stratified media, (4) lesser degrees of interference with other prominent phases (i.e., *SKS*, *ScS*, *SP*), and (5) greater efficiency in P-to-S scattering than the reverse process [see, e.g., *Wu*, 1989]. Following BR and similar studies before it, we adopt a ray theoretic Green's function for $G^{\dagger}_{in}$, that is,

$$\begin{aligned}G^{\dagger}_{in}(x_1, x_3; x_1', x_3'; x_2) = \frac{1}{\sqrt{-i\omega}}\Big\{&A^P e^{i\omega\tau^P}\hat{x}^P_i(x_3)\hat{x}^P_n(x_3')\\ &+A^S e^{i\omega\tau^S}\left[\hat{x}^{SV}_i(x_3)\hat{x}^{SV}_n(x_3') + \hat{x}^{SH}_i(x_3)\hat{x}^{SH}_n(x_3')\right]\Big\},\end{aligned} \tag{17}$$

where the phase delays τ^P, τ^S are defined by

$$\tau^P = \tau^P(x_1, x_3; x_1', x_3'; x_2) = p^P_1|x_1 - x_1'| - p_2 x_2 + q^P(x_3; x_3'), \tag{18}$$

$$\tau^S = \tau^S(x_1, x_3; x_1', x_3'; x_2) = p^S_1|x_1 - x_1'| - p_2 x_2 + q^S(x_3; x_3'), \tag{19}$$

and $A^P, A^S, q^P, q^S, \hat{x}^P_i, \hat{x}^{SV}_i, \hat{x}^{SH}_i$ are defined in Appendix A. Note that the minus sign on p_2x_2 in both (18) and (19) arises from

the definition of the adjoint Green's function. The Fourier transformation which resulted in (8) implies that u^0 in (15) represents a single harmonic component (ωp_2) of the incident wave field. As indicated earlier, we will take this wave number to characterize the incident wave field over the entire receiver array. Moreover, we shall, for the time being, ignore the effects of the free surface. The incident wave field can thus be written as

$$u_i^0(x_1, x_3; x_2) = A^0(x_3) e^{i\omega\tau^0} \hat{x}_i^0(x_3), \tag{20}$$

where

$$A^0(x_3) = 1/\sqrt{\alpha^0(x_3)\rho^0(x_3)}, \tag{21}$$

$$\tau^0 = \tau^0(x_1, x_3; x_2) = p_1^0 x_1 + p_2 x_2 + \int_0^{x_3} dy_3 p_3^0(y_3), \tag{22}$$

$$\hat{\mathbf{x}}^0(x_3) = \alpha^0(x_3)\left[p_1^0, p_2, p_3^0(x_3)\right]^{\mathrm{T}}. \tag{23}$$

The unit polarization vectors $\hat{x}_i^P, \hat{x}_i^0$ of the P waves in (17) and (20) are in the same direction as their respective slowness vectors $\partial_i\tau^P$ and $\partial_i\tau^0$. The S polarization of the Green's function in (17) is defined in terms of mutually perpendicular SV and SH unit vectors, $\hat{x}_i^{SV}$ and $\hat{x}_i^{SH}$. Note, however, that only the component of polarization (say $a^{(2)}\hat{x}_i^S$) that lies within the plane formed by the incident P ray and Green's function S ray is involved in P-to-S scattering. Therefore we make use of the S polarization convention defined by *Beylkin and Burridge* [1990] to represent this polarization locally at the scattering point. By retaining only those terms of highest order in frequency and recasting the perturbations $(\Delta\lambda, \Delta\mu, \Delta\rho)$ in $(\Delta\alpha, \Delta\beta, \Delta\rho)$ as a set of more nearly independent variables (see, e.g., BR), it follows that we may reformulate (15) in terms of scattering contributions from P and S modes:

$$\begin{aligned}\Delta\tilde{u}_n^1 = \frac{\omega^2}{\sqrt{-i\omega}} \int\int dx_1 dx_3 \rho^0 \\ \cdot\left\{2\frac{\Delta\alpha}{\alpha^0} + \frac{\Delta\beta}{\beta^0}\left[2\left(\frac{\beta^0}{\alpha^0}\right)^2(\cos 2\theta - 1)\right]\right. \\ \left. + \frac{\Delta\rho}{\rho^0}\left[1 + \cos\theta + \left(\frac{\beta^0}{\alpha^0}\right)^2(\cos 2\theta - 1)\right]\right\} \\ \cdot A^P(x_3; x_3') A^0(x_3) e^{i\omega(\tau^P + \tau^0)} \hat{x}_n^P(x_3'),\end{aligned} \tag{24}$$

$$\begin{aligned}\Delta\tilde{u}_n^2 = \frac{\omega^2}{\sqrt{-i\omega}} \int\int dx_1 dx_3\ \rho^0 \left[\frac{\Delta\beta}{\beta^0}\left(2\frac{\beta^0}{\alpha^0}\sin 2\theta\right)\right. \\ \left. + \frac{\Delta\rho}{\rho^0}\left(\sin\theta + \frac{\beta^0}{\alpha^0}\sin 2\theta\right)\right] A^S(x_3; x_3') A^0(x_3) e^{i\omega(\tau^S + \tau^0)} a^{(2)} \hat{x}_n^S(x_3'),\end{aligned} \tag{25}$$

where superscript zero denotes properties of the reference medium, θ is the "scattering" angle between incident and scattered (i.e., Green's function) rays. In (24) and (25) the scattered wave field is linearly related to the material property perturbations through θ-dependent coefficients which describe the radiation patterns for scattering interactions of P into P ($\Delta\hat{\mu}_n^1$) and P into S ($\Delta\hat{\mu}_n^2$) (see Table 1 for list of scattering modes). Since the reference plane wave field is upgoing, both interactions represent forward scattering; that is, the sampling of scattering angle will tend to be centered about $\theta = 180°$. Further note that both integrals in (24) and (25) are 2-D with no dependence on x_2. In fact, their form is similar to that outlined for the strictly 2-D in-plane analysis in BR and thus allows for an analogous development of the linearized inverse scattering operator using the generalized Radon transform [*Miller et al.*, 1987; *Beylkin and Burridge*, 1990] or related approaches [*Jin et al.*, 1992; *Forgues and Lambaré*, 1997] as we describe in section 3.

Table 1. Scattering Modes

Scattering Index q	Description	Icon[a]
1	forward scattered P-to-P	$P\uparrow\ P\uparrow$
2	forward scattered P-to-S	$P\uparrow\ S\uparrow$
3	backscattered P-to-P	$P\downarrow\ P\uparrow$
4	backscattered P-to-S	$P\downarrow\ S\uparrow$
5	backscattered S-to-P	$S\downarrow\ P\uparrow$
6	backscattered S-to-S (polarization in-plane)	$S_\parallel\downarrow\ S_\parallel\uparrow$
7	backscattered S-to-S (polarization out-of-plane)	$S_\perp\downarrow\ S_\perp\uparrow$

[a] Incident wave type and direction of propagation are indicated by first letter and arrow, while scattered wave type and direction are indicated by second letter and arrow.

3. Inverse Problem

For convenience, (24) and (25) will be recast in a more compact form as

$$\Delta\tilde{u}_n^q(\mathbf{x}', \mathbf{p}_\perp^0, \omega) = \frac{\omega^2}{\sqrt{-i\omega}} \int d\mathbf{x}\, f^q(\mathbf{x}, \theta) \mathcal{A}_n^q(\mathbf{x}, \mathbf{x}') e^{i\omega\mathcal{T}^q(\mathbf{x}, \mathbf{x}')}, \tag{26}$$

where the 2-D spatial variables $\mathbf{x}$, $\mathbf{x}'$ are understood to span the x_1, x_3 plane, index q identifies the wave type interaction, the scattering potential $f^q(\mathbf{x}, \theta)$ includes both the material property perturbations and scattering angle-dependent radiation patterns, and we have for, e.g., $q = 1$,

$$A_n^1(\mathbf{x}, \mathbf{x}') = A^0(x_3) A^P(x_3; x_3') \hat{x}_n^P(x_3') \tag{27}$$

$$\mathcal{T}^1(\mathbf{x}, \mathbf{x}') = \mathcal{T}^0(x_1, x_3; x_2) + \mathcal{T}^P(x_1, x_3, x_1', x_3'; x_2). \tag{28}$$

It will prove expedient to represent the dependence of the scattered waves on the incident wave through the two independent components of incident horizontal slowness $\mathbf{p}_\perp^0 = [p_1^0, p_2]^{\mathrm{T}}$. A new, filtered time series $v_n^q(\mathbf{x}', \mathbf{p}_\perp^0, t)$ is introduced by multiplying both sides of (26) by $i\mathrm{sgn}(\omega)/\sqrt{-i\omega}$, followed by an inverse Fourier transform,

$$\begin{aligned} v_n^q(\mathbf{x}', \mathbf{p}_\perp^0, t) &= \frac{1}{2\pi}\int d\omega e^{-i\omega t} \Delta\tilde{u}_n^q(\mathbf{x}', \mathbf{p}_\perp^0, \omega) \frac{-i\ \mathrm{sgn}(\omega)}{\sqrt{-i\omega}}, \\ &= -\int d\mathbf{x}\, f^q(\mathbf{x}, \theta) \mathcal{A}_n^q(\mathbf{x}, \mathbf{x}') \frac{1}{2\pi}\int d\omega\ i\omega e^{-i\omega[t - \mathcal{T}^q(\mathbf{x}, \mathbf{x}')]} i\ \mathrm{sgn}(\omega), \\ &= -\int d\mathbf{x}\, f^q(\mathbf{x}, \theta) \mathcal{A}_n^q(\mathbf{x}, \mathbf{x}') \mathcal{H}\{\delta'[t - \mathcal{T}^q(\mathbf{x}, \mathbf{x}')]\}, \end{aligned} \tag{29}$$

where $\mathcal{H}\{\}$ denotes Hilbert transform. Assuming that the scattering body is localized to the vicinity of a point $\mathbf{x}_0$, the final integral in (29) may be approximated following the approach of *Miller et al.* [1987, equations (19)–(25)] as

$$\begin{aligned}\int d\mathbf{x}\, f^q(\mathbf{x}, \theta) \mathcal{A}_n^q(\mathbf{x}, \mathbf{x}') \mathcal{H}\{\delta'[t - \mathcal{T}^q(\mathbf{x}, \mathbf{x}')]\} \\ \approx \frac{\mathcal{A}_n^q(\mathbf{x}_0, \mathbf{x}')}{|\nabla_0 \mathcal{T}^q|^2} \int d\mathbf{x}\, f^q(\mathbf{x}, \theta) \mathcal{H}\{\delta'[\mathbf{n}\cdot(\mathbf{x} - \mathbf{x}_0)]\}.\end{aligned} \tag{30}$$

The spatial gradient of the total travel time function $\nabla_0\mathcal{T}^q = \nabla_0\mathcal{T}^q(\mathbf{x}_0, \mathbf{x}')$ is evaluated with respect to the scatter point coordinate $\mathbf{x}_0$, and $\mathbf{n} = \nabla_0\mathcal{T}^q/|\nabla_0\mathcal{T}^q|$ is a unit vector which, note, is confined to the x_1, x_3 plane. It follows that we may approximate $v_n^q(\mathbf{x}', \mathbf{p}_\perp^0, t)$ as

$$v_n^q\left[\mathbf{x}', \mathbf{p}_\perp^0, t = \mathcal{T}^q(\mathbf{x}_0, \mathbf{x}')\right] \approx -\frac{A_n^q(\mathbf{x}_0, \mathbf{x}')}{|\nabla_0\mathcal{T}^q|^2}\int d\mathbf{x}\, f^q(\mathbf{x}, \theta)\mathcal{H}\{\delta'[\mathbf{n}\cdot(\mathbf{x}-\mathbf{x}_0)]\} \tag{31}$$

(this approximation will ultimately restrict the validity of the reconstruction algorithm to short-wavelength variations in structure [see, e.g., *Miller et al.*, 1987]). It is further convenient to take the inner product of $\mathcal{A}_n^q(\mathbf{x}_0, \mathbf{x}')$ with both sides of (31) and rearrange such that

$$\int d\mathbf{x}\, f^q(\mathbf{x}, \theta)\mathcal{H}\{\delta'[\mathrm{n}\cdot(\mathbf{x}-\mathbf{x}_0)]\} = -\frac{|\nabla_0\mathcal{T}^q|^2}{|\mathcal{A}^q|^2}\sum\nolimits_n \mathcal{A}_n^q(\mathbf{x}_0, \mathbf{x}')v_n^q\left[\mathbf{x}', \mathbf{p}_\perp^0, t = \mathcal{T}^q(\mathbf{x}_0, \mathbf{x}')\right], \tag{32}$$

where $|\mathcal{A}^q|^2 = \sum_n \mathcal{A}_n^q(\mathbf{x}_0, \mathbf{x}')\mathcal{A}_n^q(\mathbf{x}_0, \mathbf{x}')$. Equation (32) is in a form which allows us to exploit the definition of the inverse 2-D Radon transform to define a back projection operator that reconstructs the θ-dependent scattering potential $f^q(\mathbf{x}_0, \theta)$. The 2-D Radon transform pair is given by [e.g., *Deans*, 1983]

$$F(\mathbf{n}, s) = \int d\mathbf{x} f(\mathbf{x})\delta(s - \mathbf{n}\cdot\mathbf{x}) \tag{33}$$

$$\begin{aligned} f(\mathbf{x}_0) &= -\frac{1}{4\pi}\int d\mathbf{n}\ \mathcal{H}\left[\frac{\partial}{\partial s}F(\mathbf{n}\ s)\ |_{s=\mathbf{n}\cdot\mathbf{x}_0}\right] \\ &= -\frac{1}{4\pi}\int d\mathbf{n}\int d\mathbf{x}\, f(\mathbf{x})\mathcal{H}\{\delta'[\mathbf{n}\cdot(\mathbf{x}_0-\mathbf{x})]\} \\ &= -\frac{1}{4\pi}\int_0^{2\pi} d\psi\int d\mathbf{x}\, f(\mathbf{x})\mathcal{H}\{\delta'[\mathbf{n}\cdot(\mathbf{x}_0-\mathbf{x})]\} \end{aligned} \tag{34}$$

where the angle ψ defines the direction of $\mathbf{n}$ (and, in our case, $\nabla_0\mathcal{T}^q$ as shown in Figure 4). A comparison of equations (34) and (32) leads directly to an inversion formula for the scattering potential as

$$\langle f^q(\mathbf{x}_0, \theta)\rangle = \frac{1}{4\pi}\int d\psi\frac{|\nabla_0\mathcal{T}^q|^2}{|\mathcal{A}^q|^2}\cdot\sum_n \mathcal{A}_n^q(\mathbf{x}_0, \mathbf{x}')v_n^q\left[\mathbf{x}', \mathbf{p}_\perp^0, t = \mathcal{T}^q(\mathbf{x}_0, \mathbf{x}')\right], \tag{35}$$

which is valid within the high-frequency and single-scattering approximations that we have made.

Equation (35) indicates that with a suite of measurements made at constant θ and sampling the full range of ψ, one may reconstruct the scattering potential at a point $\mathbf{x}_0$ within the validity of the single-scattering and high-frequency assumptions. Isolation of the scattering potential is, of course, only an intermediate result from which we wish to extract the material property perturbations. To proceed, we must exploit the fact that our data will, in general, represent a range of scattering angles θ_i. Thus we may write

$$\langle f^q(\mathbf{x}_0, \theta_i\rangle = \sum_{r=1}^{3} W_r^q(\theta_i)\Delta m_r(\mathbf{x}_0), \tag{36}$$

where W_r^q are the θ-dependent radiation pattern coefficients in (24) and (25) and Δm_r are the material property perturbations ($\Delta\alpha/\alpha^0$, $\Delta\beta/\beta^0$, $\Delta\rho/\rho^0$ for r = 1, 2, 3). With four or more independent measurements in θ_i this linear system is overdetermined and may be solved in a least squares sense. Although the problem is solved in principle, it is desirable to recast the solution in a form more amenable to practical implementation. Specifically, we wish to identify source ($|\mathbf{p}_\perp^0|$, γ) and receiver (x'_1) coordinates as integration/summation variables in place of ψ, θ. This will require a further subdivision of the data into magnitude of the incident horizontal slowness, $|\mathbf{p}_\perp^0|$, and the solution of a weighted set of normal equations written in matrix form as

$$(\mathsf{W}^{\mathrm{T}}\mathsf{C}\mathsf{W})\Delta\mathsf{m} = (\mathsf{W}^{\mathrm{T}}\mathsf{C})\mathsf{f} = \mathsf{g}, \tag{37}$$

where the correspondences are $W_r^q(\theta_i) \leftrightarrow \mathrm{W}$, $f^q(\mathbf{x}_0, \theta_i) \leftrightarrow \mathsf{f}$, and $\Delta\mathsf{m}_r(\mathbf{x}_0) \leftrightarrow \Delta\mathsf{m}$. The weighting coefficients C_{ij} (nonzero elements of diagonal matrix C) in (37) can be chosen in a variety of ways; one possibility is to represent the elements of g as

$$\begin{aligned} g_r(\mathbf{x}_0) &= \sum_i\sum_j\sum_q C_{ij}W_r^q(\theta_i)f^q\left(\mathbf{x}_0, \theta_i, |\mathbf{p}_\perp^0|_j\right) \\ &= \frac{1}{4\pi}\int d\,|\mathbf{p}_\perp^0|\int d\theta\int d\psi\sum_q W_r^q(\theta)\frac{|\nabla_0\mathcal{T}^q|^2}{|\mathcal{A}^q|^2} \\ &\quad\cdot\sum_n \mathcal{A}_n^q(\mathbf{x}_0, \mathbf{x}')v_n^q[\mathbf{x}', \mathbf{p}_\perp^0, t = \mathcal{T}^q(\mathbf{x}_0, \mathbf{x}')], \end{aligned} \tag{38}$$

where j indexes source events.

The integration over ψ, θ in (38) is now recast to obtain an integration over event back azimuth γ and receiver position x'_1 through the introduction of a Jacobian of the corresponding transformation [*Beylkin*, 1985] (see Appendix B):

$$\begin{aligned} g_r(\mathbf{x}_0) &= \frac{1}{4\pi}\int d\,|\mathbf{p}_\perp^0|\int d\gamma\int dx'_1\left|\frac{\partial(\psi, \theta)}{\partial(x'_1, \gamma)}\right| \\ &\quad\cdot\sum_q W_r^q(\theta)\frac{|\nabla_0\mathcal{T}^q|^2}{|\mathcal{A}^q|^2}\sum_n \mathcal{A}_n^q(\mathbf{x}_0, \mathbf{x}')v_n^q\left[\mathbf{x}', \mathbf{p}_\perp^0, t = \mathcal{T}^q(\mathbf{x}_0, \mathbf{x}')\right]. \end{aligned} \tag{39}$$

Equation (39) thus defines three weighted diffraction stacks, $g_r(\mathbf{x}_0)$, of the filtered data $v_n{}^q$ along travel time curves $t = \mathcal{T}^q(\mathbf{x}_0, \mathbf{x}')$ for all sources and receivers. The material property perturbations at any image point $\mathbf{x}_0$ are retrieved from these stacks through a trivial 3 × 3 matrix inversion and multiplication as

$$\Delta\mathsf{m} = (\mathrm{W}^{\mathrm{T}}\mathsf{C}\mathsf{W})^{-1}\mathsf{g} = \mathsf{H}^{-1}\mathsf{g}, \tag{40}$$

where the elements of H are defined by

$$H_{rs}(\mathbf{x}_0) = \int d\,|\mathbf{p}_\perp^0|\int d\theta\sum_q W_r^q(\theta, |\mathbf{p}_\perp^0|, \mathbf{x}_0)W_s^q(\theta, |\mathbf{p}_\perp^0|, \mathbf{x}_0), \tag{41}$$

with the dependence of radiation pattern on $|\mathbf{p}_\perp^0|$ and $\mathbf{x}_0$ explicitly identified.

The formulation we have set out above has a number of properties that are particularly attractive in the treatment of teleseismic waves. In particular, the method can accommodate a wide variety of source-receiver geometries simultaneously and is not restricted to the treatment of data from an individual physical experiment, i.e., involving a single source. As a result, there is no formal requirement for uniform sampling in receivers x'_1, or source back azimuth γ. This feature is important when considering the irregular distribution of global seismicity and the difficulty in locating quality recording sites. Furthermore, the ray-based formulation results in an explicit identification of different scattering mode interactions q (as well as forward versus backscattering as we discuss in section 4) within the back projection formula (39). Consequently, one may monitor and weight the individual scattering mode contributions to the elastic parameter reconstruction at any image point. This consideration along with a host of other important practical issues

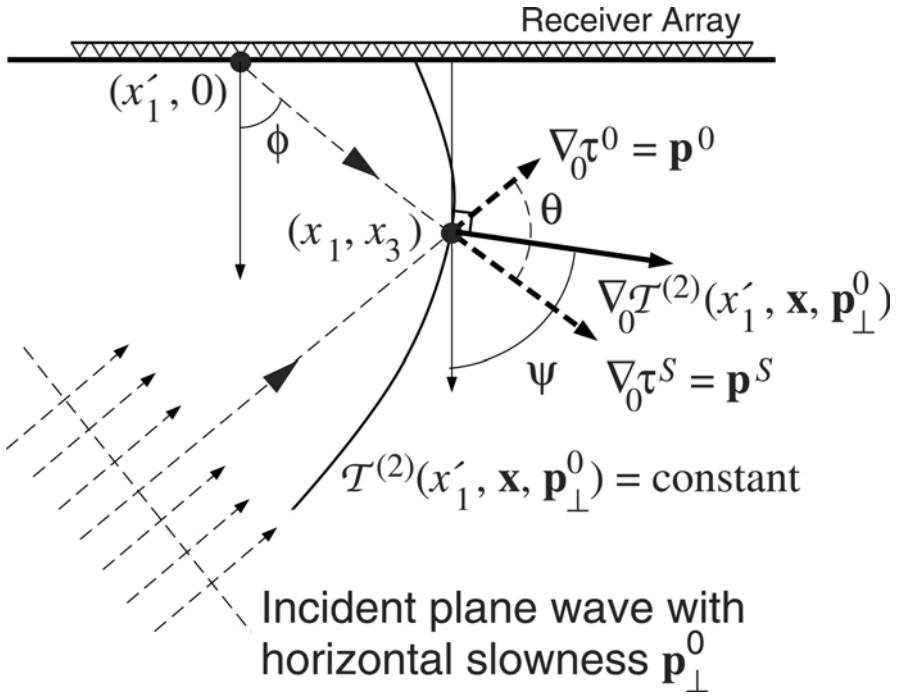

Figure 4. Geometrical quantities referred to in the text, projected onto the x_1,x_3 plane. Solid lines are quantities confined to the x_1,x_3 plane (i.e., $\nabla_0 \mathcal{T}^{(2)}(x'_1, \mathbf{x}, \mathbf{p}^0)$, ψ, ϕ), and dashed lines signify properties with a projection in x_2 (i.e., $\nabla_0 T^0$, $\nabla_0 T^S$, θ). Note that the sensitivity of total travel time to scatterer location, $\nabla_0 \mathcal{T}^{(2)}$, is perpendicular to the isochronal surface $\mathcal{T}^{(2)}$ = const.

pertaining to numerical implementation are discussed in detail in papers 2 and 3.

4. Incorporation of the Free Surface

We have, to this point, ignored the effect of the free surface, which, for the present discussion, will be taken to be planar and horizontal. The free surface impacts the problem in two ways. First, it produces *P* and *S* reflections with amplitudes comparable (though smaller) to that of the incident wave, which are subsequently backscattered by underlying lithospheric structure. Second, the free surface distorts the amplitude and polarization of the (surface) recorded displacement from those expected for a purely upgoing wave. We will investigate both of these aspects in turn.

Strong reverberations, in particular, crustal multiples, are often considered a source of noise in lithospheric studies employing teleseismic waves because they arrive in the same time interval (10–25 s) after direct *P* in which direct conversions from depths of 100–250 km are expected. In principle, however, these backscattered waves can be harnessed to place constraints on structure that are complementary to those afforded by forward scattered waves with respect to both spatial resolution and material property separation. Incorporation of backscattered waves is straightforward within the formalism and geometry that we have adopted. Since the incident *P* wave is taken to be planar (i.e., characterized by a single horizontal slowness $|\mathbf{p}_\perp^0|$), the surface-reflected waves will share the incident horizontal slowness. By including two additional terms in (20) corresponding to the free surface reflections, i.e.,

$$u_i^0(x_1, x_3; x_2) = A^0(x_3)[e^{i\omega T^0}\hat{x}_i^0(x_3) + \tilde{R}^{PP}e^{i\omega T^{PP}}\hat{x}_i^{PP}(x_3) + \tilde{R}^{SP}e^{i\omega T^{SP}}\hat{x}_i^{SP}(x_3)], \quad (42)$$

the Born approximation is improved as a greater proportion of the total wave field is accounted for within u_i^0. Another way of viewing this modification is to note that the additional terms effectively represent plane wave (*P* and *S*) sources incident from above with relative amplitudes governed by the free-surface reflection coefficients $\hat{R}^{PP}$, $\hat{R}^{SP}$. The interaction of these reflected waves with underlying structure introduces, in principle, a further four (back)scattering mode interactions (i.e., reflected *P*-to-*P* (q = 3), *P*-to-*S* (q = 4), *S*-to-*P* (q = 5), and *S*-to-*S* (q = 6,7) for a total of six phases providing constraints on subsurface elastic structure (in practice, these interactions have different sensitivities rendering some more useful than others as discussed in papers 2 and 3). The free-surface reflected *P*-to-*P* and *P*-to-*S* (q = 3,4) interactions are (with the trivial modification of amplitude by free-surface reflection coefficient) directly accounted for by the forward scattering formulation (q = 1,2) of previous sections. To accommodate incident S wave interactions (q = 5,6,7), we must incorporate the relevant radiation patterns within $W_r^q(\theta)$ for use in (39) and (41). Note that for oblique incidence this will generally require the definition of two *S*-to-*S* scattering modes: one (q = 6) that describes scattering for polarization within the plane defined by incident and Green's function rays and a second (q = 7) for polarization perpendicular to this plane. Accordingly, we write

$$\Delta\tilde{u}_n^5 = -\frac{\omega^2}{\sqrt{-i\omega}}\int\int dx_1 dx_3\ \rho^0\left[\frac{\Delta\beta}{\beta^0}\left(2\frac{\beta^0}{\alpha^0}\sin 2\theta\right) + \frac{\Delta\rho}{\rho^0}\left(\sin\theta + \frac{\beta^0}{\alpha^0}\sin 2\theta\right)\right] \cdot A^P(x_3; x_3')A^0(x_3)\tilde{R}^{SP}e^{i\omega(T^P + T^{SP})}a^{(5)}\hat{x}_n^P(x_3'), \quad (43)$$

$$\Delta\tilde{u}_n^6 = \frac{\omega^2}{\sqrt{-i\omega}}\int\int dx_1 dx_3\ \rho^0\left[\frac{\Delta\beta}{\beta^0}2\cos 2\theta + \frac{\Delta\rho}{\rho^0}(\cos\theta + \cos 2\theta)\right] \cdot A^S(x_3; x_3')A^0(x_3)\tilde{R}^{SP}e^{i\omega(T^S + T^{SP})}a^{(6)}\hat{x}_n^{S\|}(x_3'), \quad (44)$$

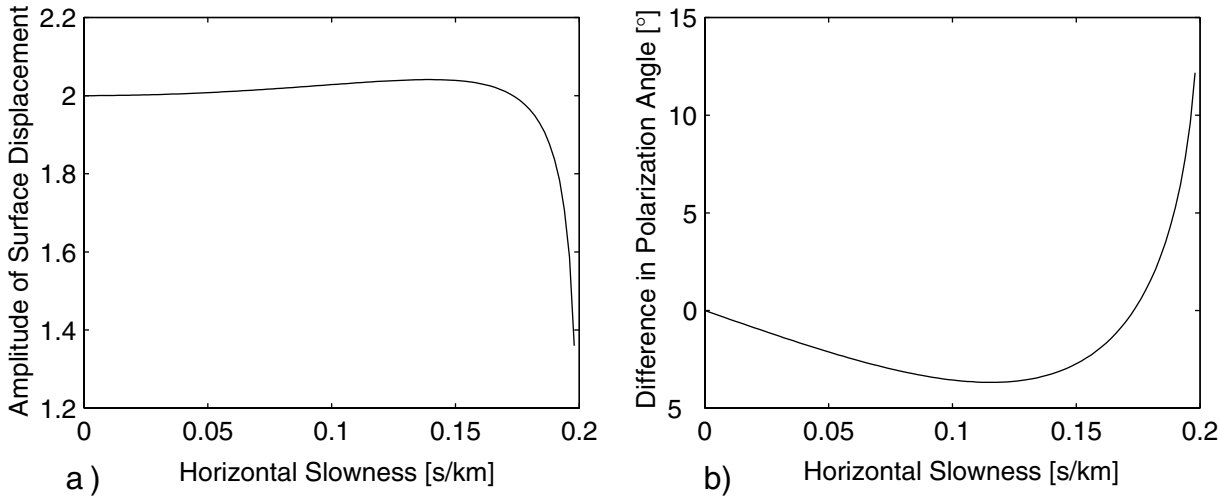

Figure 5. Free-surface response to a unit-amplitude plane wave as a function of horizontal slowness. (a) Amplitude of ground motion computed as $(F_{R\_P}^2 + F_{Z\_P}^2)^{0.5}$ in the notation of BR. (b) Difference in polarization angle between actual ground motion ($\tan^{-1}F_{R\_P}/F_{Z\_P}$) of BR) and incident wave. Both of these quantities were calculated for surface velocities of $\alpha = 5$ km/s, $\beta = 2.89$ km/s. Note that both quantities show little variation except at near-grazing incidence.

$$\Delta\tilde{u}_n^7 = \frac{\omega^2}{\sqrt{-i\omega}} \int\int dx_1 dx_3\ \rho^0 \left[\frac{\Delta\beta}{\beta^0} 2\cos\theta + \frac{\Delta\rho}{\rho^0}(1+\cos\theta) \right] \cdot\ A^S(x_3; x_3') A^0(x_3) \tilde{R}^{SP} e^{i\omega(\mathcal{T}^S + \mathcal{T}^{SP})} a^{(7)} \hat{x}_n^{S_\perp}(x_3'), \tag{45}$$

Here, as in (25), the factors $a^{(6)}\hat{x}_n^{S_\parallel}$ and $a^{(7)}\hat{x}_n^{S_\perp}(x_3')$ account for the effect of initial S wave polarization on the scattering mode amplitudes [see, e.g., *Beylkin and Burridge*, 1990]. A full list of scattering modes appears in Table 1.

In principle, we must also consider the free surface from the point of view of the recorded displacement field. Equation (39), for example, implicitly assumes that the filtered data v_n^q comprise only upgoing waves; the (reflected) downgoing P and S components are ignored. Both the recorded wave amplitudes and polarizations will therefore generally differ from those of the pure upgoing mode. These effects can be readily accounted for using the elements of the free-surface transfer matrix as defined in the appendix of BR. However, aside from a factor of 2 scaling in amplitude, the effect of the free surface is rather minor. Figure 5 displays the amplitude and direction of displacement at the free surface, as a function of horizontal slowness, for an incident P wave with unit amplitude and surface P and S velocities of 5.0 and 2.9 km/s, respectively. Over most of the slowness range, the amplitude of surface motion varies by <5%, while the polarization direction differs by less than ±5° from that of the incident wave. Thus corrections for the free surface beyond the simple factor of 2 will be significant only in very low noise circumstances.

5. Resolution

In this section we discuss several issues related to the resolution of images formed using the approach detailed above. Resolution in this context takes two distinct forms, notably the ability to isolate material property perturbations and the geometrical resolution, which includes both volume localization and dip definition. Geometrical resolution is directly assessed by defining the resolution kernel for the generalized Radon transform. Accordingly, we substitute the middle part of (29) into (35), yielding

$$\langle f^q(\mathbf{x}_0, \theta) \rangle = \int d\mathbf{x}\ R(\mathbf{x}_0, \mathbf{x}) f^q(\mathbf{x}, \theta), \tag{46}$$

where

$$R(\mathbf{x}_0, \mathbf{x}) = \frac{1}{8\pi^2} \int d\psi \int d\omega \frac{\sum_n A_n^q(\mathbf{x}_0, \mathbf{x}') A_n^q(\mathbf{x}, \mathbf{x}')}{\sum_n A_n^q(\mathbf{x}_0, \mathbf{x}') A_n^q(\mathbf{x}_0, \mathbf{x}')} \cdot\omega\ |\nabla_0 \mathcal{T}^q(\mathbf{x}_0, \mathbf{x}')|^2\ e^{-i\omega[\mathcal{T}^q(\mathbf{x}_0, \mathbf{x}') - \mathcal{T}^q(\mathbf{x}, \mathbf{x}')]} \tag{47}$$

is the resolution kernel. Evaluating this expression to leading order (i.e., setting $A_n^q(\mathbf{x}, \mathbf{x}') = A_n^q(\mathbf{x}_0, \mathbf{x}')$ and $\mathcal{T}^q(\mathbf{x}, \mathbf{x}') = \mathcal{T}^q(\mathbf{x}_0, \mathbf{x}') + \nabla_0 \mathcal{T}^q(\mathbf{x}_0, (\mathbf{x}_0, \mathbf{x}') \cdot (\mathbf{x} - \mathbf{x}_0))$, and expressing the Fourier transform along the positive real axis, we can write

$$R(\mathbf{x}_0, \mathbf{x}) = \mathrm{Re} \frac{1}{4\pi^2} \int_0^{2\pi} d\psi \int_0^{\infty} d\ |\mathbf{k}||\mathbf{k}|\ e^{-i\mathbf{k}\cdot(\mathbf{x}_0 - \mathbf{x})}, \tag{48}$$

where we have set $\mathbf{k} = \omega \nabla_0 \mathcal{T}^q(\mathbf{x}_0, \mathbf{x}')$. As written, (48) is an integral expression for the 2-D spatial delta function $\delta(\mathbf{x}_0 - \mathbf{x})$. In practical circumstances the finite aperture and limited bandwidth will result in incomplete support, and, consequently, image quality will be degraded. Typically, the degree of degradation will vary from point to point according to sampling in $\mathcal{T}^q$, and so it is desirable to compensate in some manner. One approach is to follow *de Hoop et al.* [1999] and normalize the diagonal of the resolution operator, $R(\mathbf{x}_0, \mathbf{x}_0)$ to unity, which is equivalent to replacing the factor $1/4\pi$ in (39) with a factor C, where

$$C = \frac{2\pi}{(\psi_{\max} - \psi_{\min})(|\mathbf{k}|_{\max}^2 - |\mathbf{k}|_{\min}^2)}. \tag{49}$$

In practice, we shall consider only the effect of travel time gradient in (49) and accommodate finite frequency bandwidth by normalizing each seismogram by the peak amplitude of the incident wave prior to inversion. The factor C will tend to balance amplitude anomalies across the image; however, it will not compensate for the loss in dip or volume resolution. Dip

resolution, which is discussed in greater detail by *Beylkin et al.* [1985] and *Miller et al.* [1987], is dependent on the range of ψ represented within the data set. Accordingly, dipping structures are well resolved in directions perpendicular to sampling in $\nabla_0 \mathcal{T}^q$. Volume resolution is likewise controlled by the sampling in $|\mathbf{k}| = \omega\,|\nabla_0 \mathcal{T}^q|$ and, as such, is determined in equal measure by frequency and total travel time gradient. This latter quantity is simply the sensitivity of travel time to scatterer location and, for two dimensions, appears as a quadratic weight within the back projection formula (39). Consequently (and quite naturally), contributions within the diffraction stack corresponding to scattered ray geometries that are insensitive to scatterer location are downweighted relative to those with increased sensitivity. This observation impacts the teleseismic problem in two ways. First, we note that the travel time sensitivity for forward scattering is smaller than that for backscattering owing to partial cancellation of incident and scattered slowness vectors in, e.g., (28). In fact, the sensitivity is zero in the case of intramode (e.g., *P*-to-*P*) forward scattering along the incident ray, as discussed extensively by *Marquering et al.* [1999]. The utility of incorporating the surface-reflected wave field in improving resolution thus becomes obvious (in practice, this advantage will be offset to some degree by noise as discussed in paper 3). The second issue concerns obliquity. For waves incident at oblique angles to strike the p_2 slowness components cancel in the calculation of $\nabla_0 \mathcal{T}^q(\mathbf{x}_0, \mathbf{x}')$, i.e., in (28). As a result, sensitivity is reduced for waves incident subparallel to strike, and these contributions are downweighted relative to scattering interactions that take place more nearly within the x_1, x_3 plane.

In discussing resolution we must also consider the ability to distinguish individual elastic property variations. Their resolution also depends on the ray geometries represented within particular data set and, again, differs significantly between forward scattering and backscattering. For backscattering scenarios (i.e., $\theta \approx 0°$) *P* and *S* impedances and density form the most nearly independent set of parameters, whereas *P* and *S* velocities and density are favored in forward scattering (i.e., $\theta = 180°$) configurations [see *Tarantola*, 1986; *Wu*, 1989; BR]. In more general circumstances (such as those involving both forward scattering and backscattering as here) the optimal choice must be determined through eigenvector decomposition of the Hessian matrix H in (41) and may not correspond to physical properties of interest. As demonstrated by *Forgues and Lambaré* [1997], it is possible to examine this aspect after the imaging process.

6. Concluding Remarks

In this paper, we have established a theoretical framework for inverse scattering amenable to practical inversion of the teleseismic *P* wave coda for lithospheric structure below dense, passive seismic arrays. The key elements in our development are (1) regularization of the problem through the assumption of 2-D structure to accommodate sampling requirements and current hardware inventories, (2) the assumption of plane, incident wave fields, which allows for a straightforward treatment of oblique incidence, and, consequently, the inclusion of wave fields from arbitrary back azimuths, (3) use of the generalized Radon transform as a back projection operator, which permits irregular sampling in sources and receivers, and independent consideration of different scattering mode interactions, and (4) accommodation of the backscattering response afforded by the surface-reflected wave field, which possesses greater spatial resolution than forward scattering and a complementary sensitivity to material properties. In the two companion papers we will explore a number of the practical issues surrounding implementation of the method using both synthetic seismograms and field data.

Appendix A: The 2-D Elastic Green's Function for Oblique Incidence

Our goal in this appendix is to derive a ray theoretic solution to

$$\widetilde{L}^0_{ik}\widetilde{G}_{kn} = -\delta_{in}\delta(x_1 - x_1')\delta(x_3 - x_3') \tag{A1}$$

for an isotropic 1-D reference medium. We follow the standard approach of solving (A1) exactly for a homogeneous medium and, subsequently, matching the solution to the ray theory ansatz. Solution of (A1) is, under these conditions, equivalent to solving

$$\begin{aligned}\rho(\alpha^2 - \beta^2)\partial_i\partial_j G_{jn} + \rho\beta^2\partial_j\partial_j G_{in} + \rho\omega^2 G_{in} \\ = -\delta_{in}\delta(x_1 - x_1')\delta(x_3 - x_3')e^{i\omega p_2 x_2},\end{aligned} \tag{A2}$$

where α and β are the *P* and *S* wave velocities, respectively. In (A2) we have explicitly identified the harmonic contribution in the source term and require the same dependence of G_{in}, such that

$$G_{in} = G_{in}(x_1, x_3; x_1', x_3'; x_2) = \widetilde{G}_{in}(x_1, x_3; x_1', x_3'; p_2)e^{i\omega p_2 x_2}. \tag{A3}$$

Physically, G_{in} describes the wave field originating from a line source with an axis-parallel component of forcing, that is, in the x_2 direction (see Figure A1). It is worth noting here that the amplitude of G_{in} is independent of x_2 and depends only on the distance perpendicular to the source axis. The (outgoing) solution may be determined by conventional means [*Hudson*, 1980] as

$$\begin{aligned}G_{in}(x_1, x_3; x_1', x_3'; x_2) = \frac{i}{4\rho\omega^2}\left\{\delta_{in}\frac{\omega^2}{\beta^2}\mathrm{H}_0^{(1)}(\eta r)e^{i\omega p_2 x_2}\right. \\ \left. + \partial_i\partial_n\left[\mathrm{H}_0^{(1)}(\eta r)e^{i\omega p_2 x_2} - \mathrm{H}_0^{(1)}(\nu r)e^{i\omega p_2 x_2}\right]\right\},\end{aligned} \tag{A4}$$

where $\mathrm{H}_0^{(1)}$ denotes the Hankel function of the first kind and the variables r, ν, and η are defined by

$$\begin{aligned}r = \sqrt{(x_1 - x_1')^2 + (x_3 - x_3')^2},\ \nu = \omega\sqrt{\alpha^{-2} - p_2^2}, \\ \eta = \omega\sqrt{\beta^{-2} - p_2^2}.\end{aligned} \tag{A5}$$

At high frequencies (νr, $\eta r \gg 1$) the Hankel function has the asymptotic form, e.g.,

$$\mathrm{H}_0^{(1)}(\nu r) \sim \sqrt{\frac{2}{i\pi\nu r}}e^{i\nu r}. \tag{A6}$$

Incorporating (A6) in (A4) and retaining only terms of lowest order in $r^{-1/2}$ yields the ray theoretical solution for a homogeneous medium:

$$\begin{aligned}G_{in}(x_1, x_3; x_1', x_3'; x_2) \approx \frac{i}{4\rho}\left[\sqrt{\frac{2}{i\pi\nu r}}\,p_n^P p_i^P e^{i\omega(p_1^P|x_1 - x_1'| + p_3^P|x_3 - x_3'|)}\right. \\ \left. + \sqrt{\frac{2}{i\pi\eta r}}\left(\delta_{in}p_j^S p_j^S - p_n^S p_i^S\right)e^{i\omega(p_1^S|x_1 - x_1'| + p_3^S|x_3 - x_3'|)}\right]e^{i\omega p_2 x_2},\end{aligned} \tag{A7}$$

where the superscripts *P* and *S* denote *P* and *S* waves, respectively (e.g., $p_j^S p_j^S = \beta^{-2}$), and note that $p_2{}^P = p_2{}^S = p_2$.

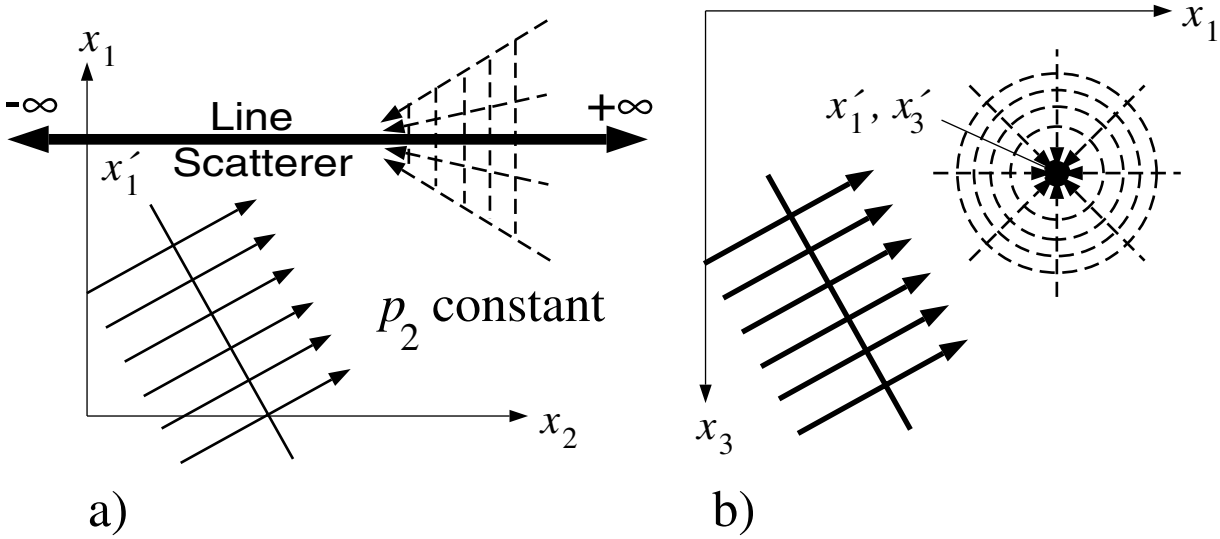

Figure A1. Schematic diagram illustrating 2-D scattering geometry for a line perturbation at x'_1, x'_3 due to an obliquely incident, plane P wave: (a) plan view and (b) depth section. Snell's law requires that the p_2 slowness component of the incident plane wave (shown as solid arrows) is preserved for all scattered waves. The adjoint Green's function (dashed arrows) thus possesses a $e^{-\omega p_2}$ dependence in x_2 but converges toward the line perturbation in the x_1, x_3 plane.

The ray theory ansatz for the Green's function of (A1) in a slowly varying, 1-D reference medium with properties $\alpha^0(x_3)$, $\beta^0(x_3)$, $\rho^0(x_3)$ is written as

$$G_{in}(x_1,x_3;x'_1,x'_3;x_2) = \frac{1}{\sqrt{-i\omega}}\Big\{A^P e^{i\omega[p_1^P|x_1-x'_1|+p_2x_2+q^P(x_3;x'_3)]} \cdot \hat{x}_i^P(x_3)\hat{x}_n^P(x'_3) + A^S e^{i\omega[p_1^S|x_1-x'_1|+p_2x_2+q^S(x_3;x'_3)]} \cdot \left[\hat{x}_i^{SV}(x_3)\hat{x}_n^{SV}(x'_3) + \hat{x}_i^{SH}(x_3)\hat{x}_n^{SH}(x'_3)\right]\Big\}. \quad \text{(A8)}$$

The vertical delay times q^P and q^S are calculated as

$$q^P(x_3;x'_3) = \int_{x'_3}^{x_3} \mathrm{d}y_3 p_3^P(y_3), q^S(x_3;x'_3) = \int_{x'_3}^{x_3} \mathrm{d}y_3 p_3^S(y_3), \quad \text{(A9)}$$

while $\hat{x}_i^P, \hat{x}_i^{SV}, \hat{x}_i^{SH}$ are unit polarization vectors defined by

$$\hat{\mathbf{x}}^P(x_3) = \alpha^0(x_3)\left[p_1^P, p_2, p_3^P(x_3)\right]^{\mathrm{T}}, \quad \text{(A10)}$$

$$\hat{\mathbf{x}}^{SV}(x_3) = \beta^0(x_3)|p_3^S(x_3)| \cdot \left[p_1^S, p_2, -(p_1^S p_1^S + p_2^2)/p_3^S(x_3)\right]^{\mathrm{T}}/\sqrt{p_1^S p_1^S + p_2^2}, \quad \text{(A11)}$$

$$\hat{\mathbf{x}}^{SH}(x_3) = (-p_2, p_1^S, 0)^{\mathrm{T}}/\sqrt{p_1^S p_1^S + p_2^2}, \quad \text{(A12)}$$

where the superscript T denotes transpose and the S wave polarization has been written in terms of SV and SH components. Note that this definition of $\tilde{x}_i^{SV}$ ensures that the reflection coefficient $\tilde{R}^{SP}$ in (42) is always negative. At the scattering point, however, we exploit an alternate polarization convention for S waves defined by *Beylkin and Burridge* [1990] to derive the compact expressions for radiation patterns in (24), (25), and (43)–(45)).

The adjoint Green's function $G_{in}^{\dagger}(x_1, x_3; x'_1, x'_3; x_2)$ required in the main derivation has the same form as (A8) but with the p_2 dependence replaced by $-p_2$. By matching (A8) with (A7) near the source point we have, for P waves,

$$A^P(x_3;x'_3;p_2) = \frac{1}{4\alpha^0(x'_3)} \cdot \sqrt{\frac{2}{\pi\rho^0(x_3)\alpha^0(x_3)\rho^0(x'_3)\left[J^P(x_3;x'_3)\right]^2\sqrt{1-p_2^2\left[\alpha^0(x'_3)\right]^2}}}, \quad \text{(A13)}$$

where the effect of obliquity is evident through the factor $\sqrt{1-p_2^2[\alpha^0(x'_3)]^2}$, and $[J^P(x_3;x'_3)]^2$ is the 2-D geometrical spreading function [e.g., *Hudson*, 1980]. This latter quantity depends on the divergence of rays in the x_1, x_3 plane as there is no divergence parallel to x_2. The amplitude function for S waves is, likewise,

$$A^S(x_3;x'_3;p_2) = \frac{1}{4\beta^0(x'_3)} \cdot \sqrt{\frac{2}{\pi\rho^0(x_3)\beta^0(x_3)\rho^0(x'_3)\left[J^S(x_3;x'_3)\right]^2\sqrt{1-p_2^2\left[\beta^0(x'_3)\right]^2}}}. \quad \text{(A14)}$$

Note that by setting $p_2 = 0$ in (A13) and (A14), we retrieve standard forms for the 2-D elastic wave Green's function.

Appendix B: Jacobian of the Transformation of Variables

In this appendix we evaluate the Jacobian, which appears in the generalized back projection operator of (39) and that transforms the integration over data space (i.e., incident waves, receivers) to an integration over the geometrical quantities θ, ψ defined in Figure 2. In order to do so, we make note of a number of important properties. First, logistical considerations may require that receivers are laid out in irregular arrays over the Earth's surface, that is, on (x'_1, x'_2, 0). However, by virtue of the symmetries created by plane wave incidence in a 2-D medium we note that a receiver response at arbitrary x'_2 can be corrected

to an equivalent response along the x_1 axis by a simple phase shift of $e^{-i\omega p_2 x'_2}$. Thus the integration over receivers is readily reduced to an integration over coordinate x'_1 (furthermore, it is generally desirable and convenient to normalize all times to the arrival of direct P; see discussion on preprocessing in BR and paper 2). The integration over plane waves (i.e., the effective source) involves two parameters which we take to be $|\mathbf{p}^0_\perp|$ and γ, where $|\mathbf{p}^0_\perp| = \sqrt{(p^0_1)^2 + (p_2)^2}$ is the magnitude of incident horizontal slowness and γ is the back azimuth to the event measured clockwise from the x_1 axis (see Figure 1). Accordingly, the integration over data space spans three independent variables ($|\mathbf{p}_\perp{}^0|$, γ, x'_1), while the imaging conditions require two independent variables: ψ for dip resolution and θ to distinguish the material property perturbations. The inequity resulting from the one additional data parameter, in principle, reflects data redundancy and, in practice, is important due to high noise levels and the sparse, irregular distribution of global seismicity. We have some liberty, therefore, in which two (of a total three) data variables we include in the Jacobian evaluation. Our choice of x'_1, γ in (39) is motivated by the fact that these two variables are generally sampled more completely than $|\mathbf{p}_\perp{}^0|$, although this will be, to some degree, dependent on the distribution of earthquake sources for a particular experiment (accordingly, we list two alternative possibilities at the end of this appendix). Further note, then, that the integration in γ may be reduced from a full 360° to a 180° interval on one side of the vertical plane oriented perpendicular to strike (i.e., the x_1, x_3 plane). This is a plane of mirror symmetry which implies that any source falling outside the 180° window can be corrected to an equivalent response within the interval by reversing the sign of the component of motion in the x_2 direction.

To proceed, we define the angular quantities θ, ψ for P-to-S scattering through

$$\cos\theta = \alpha^0\beta^0\Big[\pm|\mathbf{p}^0_\perp|\cos\gamma\sqrt{(\beta^0)^{-2} - (|\mathbf{p}^0_\perp|\sin\gamma)^2 - (p^S_3)^2} - (|\mathbf{p}^0_\perp|\sin\gamma)^2 \pm p^S_3\sqrt{(\alpha^0)^{-2} - |\mathbf{p}^0_\perp|^2}\Big] \tag{B1}$$

$$\cos\psi = \frac{\alpha^0\beta^0\left(p^S_3 \pm \sqrt{(\alpha^0)^{-2} - |\mathbf{p}^0_\perp|^2}\right)}{\sqrt{(\alpha^0)^2 + (\beta^0)^2 + 2\alpha^0\beta^0\cos\theta}}, \tag{B2}$$

where all depth-dependent quantities (i.e., α^0, β^0, and p^S_3) are evaluated at the scattering point. Corresponding expressions for, e.g., P-P scattering are obtained by substituting α^0 for β^0 and p^P_3 for p^S_3 in (B1) and (B2). The signs ($\pm$) of the radicals in (B1) and (B2) are dictated by the sign of p^S_1 (dependent in turn on the horizontal location of the receiver relative to the scattering point) and the sign of $p_3{}^0$ (which depends on whether we are concerned with forward or backscattering). In this form the functional dependencies are readily identified as

$$\theta = \theta\big(p^S_3(\gamma, x'_1), \gamma\big), \tag{B3}$$

$$\psi = \psi\big[\theta\big(p^S_3(\gamma, x'_1), \gamma\big),\ p^S_3(\gamma, x'_1)\big], \tag{B4}$$

leading to the desired Jacobian

$$\left|\frac{\partial(\psi,\theta)}{\partial(x'_1,\gamma)}\right| = \left|\frac{\partial\theta}{\partial\gamma}\frac{\partial\psi}{\partial x'_1} - \frac{\partial\theta}{\partial x'_1}\frac{\partial\psi}{\partial\gamma}\right| = \left|\frac{\partial\theta}{\partial\gamma}\Big|_{p^S_3}\frac{\partial\psi}{\partial p^S_3}\Big|_\theta\frac{\partial p^S_3}{\partial x'_1}\right|. \tag{B5}$$

Evaluation of the first two quantities on the right hand side yields

$$\left.\frac{\partial\theta}{\partial\gamma}\right|_{p^S_3} = \frac{\alpha^0\beta^0 p_2}{\sin\theta\, p^S_1}(p^0_1 + p^S_1)^2 \tag{B6}$$

$$\left.\frac{\partial\psi}{\partial p^S_3}\right|_\theta = -\frac{1}{p^0_1 + p^S_1} \tag{B7}$$

The third factor, $\partial p^S_3/\partial x'_1$, can be related to the geometrical spreading function $(J^S)^2$, which is used in the calculation of amplitudes in (A14) as

$$\frac{\partial p^S_3}{\partial x'_1} = p^S_1\frac{\cos\phi}{(J^S)^2}. \tag{B8}$$

Combining (B6), (B7), and (B8), we have

$$\left|\frac{\partial(\psi,\theta)}{\partial(x'_1,\gamma)}\right| = \left|\frac{\alpha^0\beta^0\cos\phi p_2(p^0_1 + p^S_1)}{(J^S)^2\sin\theta}\right|. \tag{B9}$$

As before, the corresponding quantity for P-P scattering is readily obtained by substituting α^0 for β^0 and P superscripts for S superscripts.

Finally, it is worthwhile considering two alternatives to the Jacobian derived above. Should the distribution of seismicity be confined to one or several dominantly azimuthal corridor(s), it may be desirable to exchange the roles of $|\mathbf{p}^0_\perp|$ and γ within the back projection operator in (39). In that case an analogous development leads to the required Jacobian

$$\left|\frac{\partial(\psi,\theta)}{\partial(x'_1,|\mathbf{p}^0_\perp|)}\right| = \left|\frac{\alpha^0\beta^0\cos\theta p^S_1}{(J^S)^2\sin\theta(p^0_1 + p^S_1)}\left[\frac{p^0_1(p_2)^2}{p^S_1|\mathbf{p}^0_\perp|} - \frac{p^S_1 p^0_1}{|\mathbf{p}^0_\perp|} + 2\frac{(p_2)^2}{|\mathbf{p}^0_\perp|} + \frac{p^S_3|\mathbf{p}^0_\perp|}{p^0_3} + \frac{p^S_3 p^0_1|\mathbf{p}^0_\perp|}{p^S_1 p^0_3} - |\mathbf{p}^0_\perp|\right]\right|. \tag{B10}$$

Alternatively, if plane wave sources are only sparsely sampled as, for example, in the case of a single source recorded on an array, it may be more reasonable to limit structural recovery to a single material parameter. The optimal choice of parameter can be facilitated through a diagonalization of the Hessian matrix in (41) [*Forgues and Lambaré*, 1997; BR] upon consideration of the contributing scattering modes. In this situation we no longer need to consider scattering angle θ in the transformation of variables, and the Jacobian reduces to a simple derivative

$$\left|\frac{\partial\psi}{\partial x'_1}\right| = \left|\frac{\cos\theta}{(J^S)^2(p^0_1 + p^S_1)}\left[\frac{(p^S_3 + p^3_0)(p^S_3 p^0_1 - p^0_3 p^S_1)}{|\nabla_0\mathcal{T}^S|^2} + p^S_1\right]\right|, \tag{B11}$$

where

$$|\nabla_0\mathcal{T}^S| = \frac{\sqrt{(\alpha^0)^2 + (\beta^0)^2 + 2\alpha^0\beta^0\cos\theta}}{\alpha^0\beta^0}. \tag{B12}$$

Notation

A^0, A^P, A^S	geometrical amplitudes of incident wave and Green's function
$\mathcal{A}^q_n$	product of geometrical amplitudes and polarization for mode q
α^0, β^0, ρ^0	P and S velocities and density in the reference medium.
$\Delta\alpha$, $\Delta\beta$, $\Delta\rho$	perturbations in P and S velocities, and density.
c_{ijkl}, ρ	elasticity tensor and density.
Δc_{ijkl}, $\Delta\rho$	perturbations in elasticity tensor and density.
G_{in}	elastic wave Green's function.
g_r, g	diffraction stack vector.
f^q, f	scattering potential vector.
H_{rs}, H	Hessian matrix.
$\mathcal{H}\{\}$	Hilbert transform.
L^0_{ik}, L_{ik}	wave equation operators for the reference and true media.

λ, μ	Lamé parameters.
$\Delta\lambda$, $\Delta\mu$	perturbations in Lamé parameters.
Δm_r, $\Delta\mathsf{m}$	material property perturbation vector.
p_i^0, p_i^P, p_i^S	slowness vectors of incident wave and Green's function.
$\mathbf{p}_\perp^0$, γ	incident horizontal slowness vector and back azimuth.
ϕ	ray angle at the surface.
q	scattering mode index (see Table 1).
q^0, q^P, q^S	depth-integrated, vertical slownesses of incident wave and Green's function.
r	material property index.
$R(\mathbf{x}_0, \mathbf{x})$	resolution kernel.
$\widetilde{R}^{PP}$, $\widetilde{R}^{SP}$	free-surface reflection coefficients.
τ^0, τ^P, τ^S	travel times of incident wave and Green's function.
$\mathcal{T}^q$	sum of travel times for mode q.
$\nabla_0\mathcal{T}^q$	spatial gradient of $\mathcal{T}^q$ with respect to $\mathbf{x}_0$.
θ, ψ	scattering angle and dip angle of $\nabla_0\mathcal{T}^q$.
u_i^0, u_i, Δu_i	reference, true, and perturbation displacement wave fields.
v_i^q	filtered displacement wave field due to scattering mode q.
W_r^q, W	radiation pattern matrix.
ω, t	radial frequency and time.
$\mathbf{xp}$, $\mathbf{x}_0$	receiver and scattering point coordinates.
$\hat{\mathbf{x}}^P$, $\hat{\mathbf{x}}^{SV}$, $\hat{\mathbf{x}}^{SH}$	unit polarization vectors for *P*, *SV*, and *SH* waves.
$\hat{x}^{S_\parallel}$, $\hat{x}^{S_\perp}$	unit *S* polarization vectors for in-plane and out-of-plane scattering.
superscript†	quantity associated with adjoint wave equation.
superscript^0	quantity associated with reference medium.
overlying $\sim$	quantity Fourier transformed in x_2.

Acknowledgments. We are grateful to referees Guust Nolet and Gary Pavlis and Associate Editor Justin Revenaugh for helpful suggestions which improved presentation of the manuscript. This research was supported by NSERC (Natural Sciences and Engineering Research Council of Canada) research grant OGP0138004.

References

Aki, K., A. Christofferson, and E. S. Husebye, Determination of the three-dimensional seismic structure of the lithosphere, *J. Geophys. Res.*, *82*, 277–296, 1977.

Beylkin, G., Imaging of discontinuities in the inverse scattering problem by inversion of a causal generalized Radon transform, *J. Math. Phys.*, *26*, 99–108, 1985.

Beylkin, G., and R. Burridge, Linearized inverse scattering problems in acoustics and elasticity, *Wave Motion*, *12*, 15–52, 1990.

Beylkin, G., M. Oristaglio, and D. Miller, Spatial resolution of migration algorithms, in *Acoustical Imaging*, vol. 14, edited by A. J. Berkhout, J. Ridder, and L. F. van der Waal, pp. 155–167, Plenum, New York, 1985.

Bostock, M. G., and S. Rondenay, Migration of scattered teleseismic body waves, *Geophys. J. Int.*, *137*, 732–746, 1999. (Corrigendum to "Migration of scattered teleseismic body waves", *Geophys. J. Int.*, 139, 597, 1999.)

Chapman, C. H., The Earth flattening transformation in body wave theory, *Geophys. J. R. Astron. Soc.*, *35*, 55–70, 1973.

Deans, S. R., *The Radon Transform and Some of Its Applications*, 289 pp., John Wiley, New York, 1983.

de Hoop, M. V., C. Spencer, and R. Burridge, The resolving power of seismic amplitude data: An anisotropic inversion/migration approach, *Geophysics*, *64*, 852–873, 1999.

Dueker, K. G., and A. F. Sheehan, Mantle discontinuity structure from midpoint stacks of converted *P* to *S* waves across the Yellowstone hot spot track, *J. Geophys. Res.*, *102*, 8313–8327, 1997.

Forgues, E., and G. Lambaré, Parameterization study for acoustic and elastic ray+Born inversion, *J. Seismol. Explor.*, *6*, 253–277, 1997.

Hudson, J. A., *The Excitation and Propagation of Elastic Waves*, 225 pp., Cambridge Univ. Press, New York, 1980.

Humphreys, E. D., and K. G. Dueker, Western U. S. upper mantle structure, *J. Geophys. Res.*, *99*, 9615–9634, 1994.

Jin, S., R. Madariaga, J. Virieux, and G. Lambaré, Two-dimensional asymptotic iterative elastic inversion, *Geophys. J. Int.*, *108*, 575–588, 1992.

Kosarev, G., R. Kind, S. V. Sobolev, X. Yuan, W. Hanka, and S. Oreshin, Seismic evidence for a detached Indian lithospheric mantle beneath Tibet, *Science*, *283*, 1306–1309, 1999.

Langston, C. A., Structure under Mount Rainier, Washington, inferred from teleseismic body waves, *J. Geophys. Res.*, *84*, 4749–4762, 1979.

Levander, A., E. Humphreys, G. Ekstrom, A. Meltzer, and P. Shearer, Proposed project would give unprecedented look under North America, *Eos Trans. AGU*, *80*, 245, 1999.

Li, X.-Q., and J. L. Nabelek, Deconvolution of teleseismic body waves for enhancing structure beneath a seismometer array, *Bull. Seismol. Soc. Am.*, *89*, 190–201, 1999.

Marquering, H., F. A. Dahlen, and G. Nolet, Three-dimensional sensitivity kernels for finite-frequency traveltimes: The banana-doughnut paradox, *Geophys. J. Int.*, *137*, 805–815, 1999.

Miller, D., M. Oristaglio, and G. Beylkin, A new slant on seismic imaging: Migration and integral geometry, *Geophysics*, *52*, 943–964, 1987.

Revenaugh, J., A scattered-wave image of subduction beneath the Transverse Ranges, *Science*, *268*, 1888–1892, 1995a.

Revenaugh, J., The contribution of topographic scattering to teleseismic coda in southern California, *Geophys. Res. Lett.*, *22*, 543–546, 1995b.

Rondenay, S., M. G. Bostock, and J. Shragge, Multiparameter two-dimensional inversion of scattered teleseismic body waves, 3, Application to CASC93, *J. Geophys. Res.*, this issue.

Ryberg, T., and M. Weber, Receiver function arrays: A reflection seismic approach, *Geophys. J. Int.*, *141*, 1–11, 2000.

Shearer, P. M., M. P. Flanagan, and M. A. H. Hedlin, Experiments in migration processing of *SS* precursor data to image upper mantle discontinuity structure, *J. Geophys. Res.*, *104*, 7229–7242, 1999.

Shragge, J., M. G. Bostock, and S. Rondenay, Multiparameter two-dimensional inversion of scattered teleseismic body waves, 2, Numerical examples, *J. Geophys. Res.*, this issue.

Tarantola, A., A strategy for nonlinear elastic inversion of seismic reflection data, *Geophysics*, *51*, 1893–1903, 1986.

VanDecar, J. C., Upper-mantle structure of the Cascadia subduction zone from non-linear teleseismic travel-time inversion, Ph.D. thesis, Univ. of Wash., Seattle, 1991.

Vinnik, L. P., Detection of waves converted from *P* to *SV* in the mantle, *Phys. Earth Planet. Inter.*, *15*, 39–45, 1977.

Wu, R.-S., The perturbation method in elastic wave scattering, *Pure Appl. Geophys.*, *131*, 605–637, 1989.

M. G. Bostock, Department of Earth and Ocean Sciences, University of British Columbia, 129-2219 Main Mall, Vancouver, British Columbia, Canada V6T 1Z4. (bostock@geop.ubc.ca)

S. Rondenay, Department of Geological Sciences, Brown University, Dept. Box 1846, Providence, RI 02912, USA. (rondenay@emma.geo.brown.edu)

J. Shragge, Hager GeoScience Inc., 596 Main Street, Woburn, MA 01801, USA.

(Received July 19, 2000; revised March 14, 2001;
accepted June 9, 2001.)